European Journal of Mechanics / A Solids 120 (2026) 106264

Contents lists available at ScienceDirect

European Journal of Mechanics / A Solids

journal homepage: www.elsevier.com/locate/ejmsol

Full length article

Control of a shape memory von mises structure by an intelligent sliding mode approach ☆

Philippe Eduardo de Medeiros [a], Marcelo Amorim Savi [b], Wallace Moreira Bessa [c],*

[a] Universidade Federal do Rio Grande do Norte, Faculty of Engineering, Letters and Social Sciences of Seridó, Currais Novos, RN, 59380-000, Brazil
[b] Universidade Federal do Rio de Janeiro, COPPE - Mechanical Engineering, Center for Nonlinear Mechanics, Rio de Janeiro, RJ, 21941-594, Brazil
[c] University of Turku, Department of Mechanical and Materials Engineering, Turku, FI-20014, Finland

ARTICLE INFO

Keywords:
Sliding mode control
Neural network
Smart structures
Von mises structure
Shape memory alloy

ABSTRACT

This study presents a novel approach for active vibration control of a Shape Memory Alloy (SMA) von Mises structure using a bioinspired controller. A constitutive model that accurately captures the SMA thermomechanical behavior is used to describe the system dynamics. Nevertheless, this model is computationally demanding and requires the identification and adjustment of a large number of parameters, making its direct use in the controller design impractical for real-time control applications. In this context, the controller is based on the sliding mode control approach being enhanced with a neural network to compensate uncertainties and external disturbances, and it is designed using a polynomial constitutive model to approximate the system dynamics, as required by the control formulation. This model is adopted due to its simplicity and reduced number of parameters to be identified, while providing an approximate representation of the plant. Hence, the proposed control law is capable of predicting the system's dynamical behavior, adapting to changes, and learning from the system–environment interaction in an online manner. The closed-loop system's convergence is analyzed using a Lyapunov-like stability analysis, and numerical simulations demonstrate the effectiveness of the proposed strategy for suppressing undesired vibrations in the presence of nonlinear effects and model mismatch. Overall, the proposed approach combines reduced computational complexity with online adaptation capabilities, providing an efficient framework for active vibration control of SMA structures.

1. Introduction

Stability of structures represents a fundamental problem in mechanics, which must be studied to ensure the safety of structures against undesirable behaviors and collapses. In structural analysis, it is common to use simple dynamic models with one or two degrees of freedom (DOF) to study the fundamental characteristics of a system, as pointed out by Bazant and Cedolin (2010). These models are usually employed to investigate general aspects of the structural dynamics, providing a global comprehension of the system behavior without the superfluous complexity of more detailed models (Orlando et al., 2018; Santana et al., 2019). The well-known von Mises structure, or two-bar truss, is a popular system used for stability analysis. This structure exhibits snap-through behavior, where there are two possible displacement configurations for a given load level. This behavior is a classical example of geometric nonlinearity, where the equilibrium path goes from one stable point to another new stable point with an increasing load. Understanding the behavior of the von Mises structure is important for understanding the stability of framed structures and flat arches, as well as other physical phenomena associated with bifurcation buckling (Pelliciari and Tarantino, 2020; Falope et al., 2021; Chi et al., 2022). The simplicity of the model makes it a useful tool for analyzing these types of systems and gaining insight into their behavior. In the context of control design, simplified structural models are commonly adopted to support the development and evaluation of new control strategies, since excessive model complexity may introduce additional dynamics that make it difficult to identify the dominant system behavior and to accurately evaluate controller performance.

Shape memory structures are a class of systems that have the ability to adapt to environmental changes by altering their physical and geometrical properties through the application of an external excitation. These structures typically incorporate Shape Memory Alloys (SMAs) either embedded within or as surface layers, and utilize a combination of sensing, control, and actuation functions to achieve their intended purpose (Qian et al., 2016; Nespoli et al., 2017; Niu and Chen, 2021;

☆ This article is part of a Special issue entitled: 'Rega's 80th Birthday' published in European Journal of Mechanics / A Solids.

* Corresponding author.
E-mail addresses: philippe.medeiros@ufrn.br (P.E. de Medeiros), savi@mecanica.coppe.ufrj.br (M.A. Savi), wallace.moreirabessa@utu.fi (W.M. Bessa).

https://doi.org/10.1016/j.euromechsol.2026.106264
Received 7 April 2026; Received in revised form 9 June 2026; Accepted 21 June 2026
Available online 25 June 2026

Zheng et al., 2021; Zhang et al., 2022a). SMAs belong to a larger group of smart materials, which also includes piezoelectric materials, magnetorheological fluids, photovoltaic materials, thermoelectric materials and magnetostrictive materials. Among the various smart materials, SMAs have emerged as a preferred option for vibration control due to their exceptional energy dissipation capabilities, as well as their ability to perform well in scenarios that require large forces, strains, and low-frequency structural control (Attanasi and Auricchio, 2011).

The specific characteristics of SMAs have garnered significant attention from both scientific and engineering communities. These materials are typically utilized in applications that involve either thermal or mechanical loadings, which induce phase transformations that give rise to their unique properties (Mohd Jani et al., 2017; Karakalas et al., 2019). One of the most notable characteristics of SMAs is their ability to revert to a prior shape or dimension when subjected to an appropriate thermomechanical process, known as the shape memory effect (SME). This process is characterized by complete strain recovery accompanied by a large hysteresis loop in a loading-unloading cycle. SMAs also possess significant internal damping and superelasticity behavior, which are characterized by large nonlinear elastic strains. These exceptional properties have led to SMAs being employed as functional materials in a broad range of applications in various fields of science and engineering (Mohd Jani et al., 2014). Some of the most common applications of SMAs include use in biomedical devices (Auricchio et al., 2021), actuators (Copaci et al., 2020), micromanipulators (AbuZaiter et al., 2016), aerospace technology (Exarchos et al., 2018; Gantz et al., 2022), civil and mechanical engineering (Suhail et al., 2021; Song et al., 2022; Parmar and Mishra, 2022), among others (Chaudhari et al., 2021; Brotzu et al., 2021).

It is interesting to note that the study of smart structures, particularly those incorporating SMAs, has received considerable attention in the field of structural engineering (Sohn et al., 2023). The use of SMAs in structural design has the potential to improve the performance and efficiency of structures, by enabling them to respond to changes in their environment or loads in a controlled and predictable manner (Alves et al., 2018; Lü et al., 2021; Zhang et al., 2022b). The behavior of SMA structures can exhibit a range of dynamic responses, including periodic, quasi-periodic, and chaotic motions (Savi et al., 2002; Savi and Nogueira, 2010; Costa et al., 2019). The constitutive models used to describe the thermomechanical behavior of SMAs are critical in predicting the dynamic response of these structures. From a control design perspective, models adopted for numerical simulations and those employed in controller formulation may serve different purposes and therefore present different levels of complexity. Thus, in this work, different modeling approaches are adopted depending on whether the objective is numerical simulation or controller formulation, as will be shown in the sequel.

Some authors have investigated the control of smart structures, specifically focusing on SMA von Mises trusses. Bessa et al. (2013) introduced an effective adaptive fuzzy sliding mode controller for vibration suppression in an SMA von Mises truss. However, the polynomial constitutive model employed both in the plant representation and in the controller formulation failed to properly capture the SMA hysteretic behavior. De Paula et al. (2014) proposed a control strategy based on the time-delayed feedback method to manage chaotic responses in an SMA two-bar truss. Although effective, this method is mainly focused on chaos control that has specific characteristics as discussed by de Paula and Savi (2011). Similarly, Costa et al. (2019) investigated chaos and bifurcation control in an SMA two-bar truss using time-delayed feedback control. They exploited SMA adaptive behavior but, like Bessa et al. (2013), utilized a polynomial constitutive model that does not encompass crucial SMA phenomena.

Recent investigations have explored advanced analytical, numerical, and intelligent computational approaches for nonlinear structural systems and complex materials, including finite element formulations, multilayer perceptron-based strategies, and nonlinear dynamic analyses (Lezgy-Nazargah et al., 2025; Sekban et al., 2025; Yaylacı et al., 2025; Yazıcıoğlu et al., 2025). These studies highlight the growing interest in computationally efficient methodologies capable of dealing with nonlinearities and complex dynamic behavior in structural systems. Furthermore, they reinforce the importance of developing robust numerical and computational approaches for systems exhibiting strong nonlinear responses and parameter-dependent behavior.

This paper presents the application of an intelligent controller to control the vibration of a shape memory alloy von Mises structure. The controller employs a sliding mode control technique and is reinforced with an adaptive neural network to increase the ability to handle external disturbances and modeling inaccuracies. In addition, the controller is designed to accommodate both prior and acquired information about the system being controlled. To obtain the prior knowledge of the system dynamics, a simplified polynomial model (Falk, 1980) is used. This model can describe the thermomechanical behavior of the SMA bars with a single equation and is therefore adopted as prior knowledge in the controller design. However, to simulate the thermomechanical behavior of the real structure bars and properly capture essential SMA phenomena, such as the hysteresis loop, a more realistic constitutive model (Paiva et al., 2005), which provides close agreement with experimental data, is considered. The direct use of this constitutive model in the controller design would significantly increase the complexity of the control law and hinder its practical implementation. For this reason, a simplified polynomial model is employed in the controller, while a neural network is used to approximate the remaining dynamics and uncertainties, providing a posteriori knowledge through online learning via interaction with the system. This strategy results in a simpler control law and is enabled by the learning capability of the intelligent controller, which compensates for neglected nonlinear and hysteretic effects introduced by the discrepancy between the controller model and the plant dynamics. Therefore, the proposed approach combines reduced computational complexity with online adaptation capabilities for vibration control of an SMA von Mises structure subjected to chaotic motions.

Regarding the intelligent scheme, the controller is designed with a reduced structural complexity. A single hidden layer neural network is adopted, and its weights are updated online through interaction with the system, allowing the controller to adapt to uncertainties and external disturbances in real time. Moreover, in order to limit the network size and computational cost, the sliding surface is employed as the single input variable, rather than the full state vector. These design choices are consistent with the sliding mode framework and aim at achieving an effective balance between robustness, adaptability, reduced approximation dimensionality, and practical implementability.

Therefore, the proposed strategy offers several advantages, including (i) the possibility of using simpler constitutive models for controlling systems with complex dynamic behaviors, (ii) robustness to uncertain parameters, unmodeled dynamics, and external excitations, (iii) the ability to approximate uncertainties and external disturbances of the system with a single hidden layer, in an online way, and (iv) the adoption of a single variable as the input of the neural network. These attributes, when combined with the first two, allow the smart controller to be directly implemented in real-world industrial applications. Following the control design, the convergence properties are mathematically proven through a Lyapunov-like stability analysis, and numerical simulations are conducted to demonstrate the effectiveness and intelligence of the control strategy in the vibration control of SMA structures.

It is important to highlight that SMA properties are not being considered here for control purposes. Instead, the intelligent vibration control of the shape memory structure is accomplished by integrating an external actuator, a controller, and system state vector information. The state vector is fed into the intelligent controller, which calculates the desired control signal and sends it to the actuator. This approach is commonly used in distinct applications, including aerospace systems such as self-erectable structures and stabilization mechanisms (Savi et al., 2008; Savi, 2015).

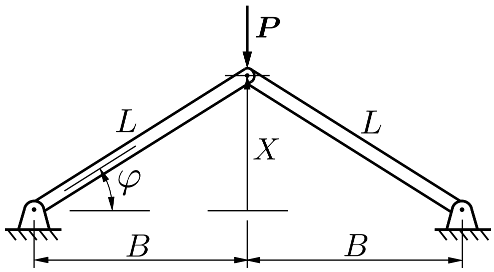

Fig. 1. Schematic representation of a von Mises structure.

2. Dynamic model

The von Mises structure studied in this paper is made of shape memory alloy, and each bar can present shape memory and superelastic effects. Due to the combination of geometric and constitutive nonlinearities, the system's nonlinear dynamics become increasingly complex. This structure is basically composed of two identical bars with same length L, same cross-section A_s and horizontal projection B, and form the same angle φ with its supports plane, as shown in Fig. 1. The mass of the structure m is considered to be concentrated at the central joint, which is constrained to move only vertically, and the critical Euler load of both bars is assumed to be sufficiently large to prevent buckling in this case. The bars are free to rotate around their supports and at the central joint.

Under these assumptions, only vertical and symmetric motions are considered, allowing the structure can be treated as a single DOF system. According to the balance of momentum, the system dynamics is expressed through the following equation of motion:

$$-2F\sin\varphi - c\dot{X} + P = m\ddot{X}\,, \tag{1}$$

where F is the force in each bar, which is related to the mechanical behavior of the structure material, c is an equivalent coefficient damping for the structure, P is an external excitation and X represents the vertical and symmetric displacement of the central joint, as shown in Fig. 1.

According to the structure arrangement, the axial bars strain is related to the angle φ by the geometrical relation:

$$\varepsilon = \frac{L}{L_0} - 1 = \frac{\cos\varphi_0}{\cos\varphi} - 1\,, \tag{2}$$

with L_0 and φ_0 representing the nominal values of L and φ, respectively.

The thermomechanical description of SMAs has been the subject of extensive research, and various constitutive theories have been proposed to understand and model their behavior. Paiva and Savi (2006), Lagoudas (2008) and Cisse et al. (2016) have contributed to the field by presenting a general overview of the research efforts associated with the thermomechanical description of SMAs. Here, the constitutive model presented by Paiva et al. (2005) is employed. Although this proposed model captures the general thermomechanical behavior of the SMAs, there are several simpler alternatives with limited capability to represent hysteretic effects. In this regard, the polynomial model proposed by Falk (1980) is also presented, which offers a simplified constitutive representation with reduced modeling complexity, making it suitable for controller design. On this basis, both models are presented and compared in the sequel, establishing the equations of motion and the responses associated with each one of them. The implications of this choice are discussed as the modeling and control formulations are developed.

2.1. Constitutive model by Paiva et al. (2005)

A constitutive model proposed by Paiva et al. (2005) is employed to describe the thermomechanical behavior of SMAs. This model is able to capture the general thermomechanical behavior of SMAs, presenting close agreement with experimental data. It can describe the main phenomena related to SMAs, such as: shape memory effect, superelasticity, plasticity, internal subloops, tensile-compressive asymmetry, among others. Nevertheless, plasticity and tensile-compressive asymmetry are not taken into account in the present work. Three state variables, given by β_1, β_2 and β_3, are considered to characterize the volume fractions of macroscopic phases, such that β_1 is associated with detwinned martensite induced by tensile stress $(M+)$, β_2 is associated with detwinned martensite induced by compressive stress $(M-)$ and β_3 is associated with austenite (A). A fourth phase β_4 is also considered, which is related to twinned martensite, and can be obtained from the phase coexistence condition, given by:

$$\beta_4 = 1 - (\beta_1 + \beta_2 + \beta_3)\,. \tag{3}$$

Considering ε and T as the strain and temperature of the structural bars, respectively, the normal stress σ and the volume fractions of macroscopic phases are described by the following set of equations:

$$\sigma = E\varepsilon + \left[\alpha + E\alpha_h\right]\left(\beta_2 - \beta_1\right) - \kappa\left(T - T_0\right), \tag{4}$$

$$\begin{aligned}\dot{\beta}_1 = \frac{1}{\eta_1}\,\{\ &\alpha\varepsilon + \sigma_M + [2\alpha_h\alpha + E\alpha_h^2](\beta_2 - \beta_1) + \\ &\alpha_h[E\varepsilon - \kappa(T - T_0)] - \partial_1 J_\pi\ \} + \partial_1 J_\chi\,,\end{aligned} \tag{5}$$

$$\begin{aligned}\dot{\beta}_2 = \frac{1}{\eta_2}\,\{\ &-\alpha\varepsilon + \sigma_M - [2\alpha_h\alpha + E\alpha_h^2](\beta_2 - \beta_1) + \\ &-\alpha_h[E\varepsilon - \kappa(T - T_0)] - \partial_2 J_\pi\ \} + \partial_2 J_\chi\,,\end{aligned} \tag{6}$$

$$\begin{aligned}\dot{\beta}_3 = \frac{1}{\eta_3}\,\{\ &0.5(E_M - E_A)[\varepsilon + \alpha_h(\beta_2 - \beta_1)]^2 + \\ &(\kappa_A - \kappa_M)(T - T_0)[\varepsilon + \alpha_h(\beta_2 - \beta_1)] + \\ &\sigma_A - \partial_3 J_\pi\ \} + \partial_3 J_\chi\,,\end{aligned} \tag{7}$$

where the horizontal width of the material's hysteresis loop on the stress–strain diagram is related to α_h, while its vertical length is controlled by α. Phase transformation dissipation, represented by η_i $(i = 1, 2, 3)$, can be defined based on the characteristics of the transformation kinetics during loading and unloading processes. Different values of η_i can be considered for loading and unloading, denoted by η_i^L and η_i^U, respectively. The material's elastic modulus E and thermal expansion coefficient κ are defined as functions of its austenitic and martensitic phases: $E = E_M + \beta_3(E_A - E_M)$ and $\kappa = \kappa_M + \beta_3(\kappa_A - \kappa_M)$, where M refers to the martensitic phase and A refers to austenite.

The terms $\partial_i J_\pi$ $(i = 1, 2, 3)$ represent the sub-differentials of the indicator function $J_\pi(\beta_1, \beta_2, \beta_3)$ with respect to β_i (Rockafellar, 1970). This function is associated with the convex set π, which imposes internal constraints on the phases' coexistence, given by $\pi = \{\beta_i \in \mathbb{R} \mid 0 \le \beta_i \le 1; \beta_1 + \beta_2 + \beta_3 = 1\}$. Similarly, the terms $\partial_i J_\chi$ $(i = 1, 2, 3)$ are sub-differentials of the indicator function $J_\chi(\dot{\varepsilon}, \dot{T}, \dot{\beta}_1, \dot{\beta}_2, \dot{\beta}3)$ with respect to $\dot{\beta}i$ (Rockafellar, 1970). The convex set χ is associated with conditions that describe internal subloops due to incomplete phase transformations (Savi and Paiva, 2005), as well as restrictions on impossible phase transformations, such as detwinned martensite into twinned martensite. Finally, the sub-differentials $\partial_i J_\pi$ and $\partial_i J_\chi$ can be interpreted as Lagrange multipliers, equivalent to projections of the phase fractions onto the volume fractions space.

Considering linear temperature dependent functions for the parameters σ_M and σ_A, which are related to stress level for phase transformation, the following equations can be defined:

$$\sigma_M = \begin{cases} -l_0 + \dfrac{l}{T_M}(T - T_M) & \text{if} \quad T > T_M\,, \\ -l_0 & \text{if} \quad T \le T_M\,, \end{cases} \tag{8}$$

$$\sigma_A = \begin{cases} -l_0^A + \dfrac{l^A}{T_M}(T - T_M) & \text{if} \quad T > T_M\,, \\ -l_0^A & \text{if} \quad T \leq T_M\,, \end{cases} \tag{9}$$

where T_M is the temperature below which the martensitic phase becomes stable for a stress free state, and l_0, l, l_0^A and l^A are parameters related to critical stress for phase transformation. The temperature T_0 present in Eqs. (4)–(7), is a reference temperature when the strain vanishes in a stress-free state ($\varepsilon = 0$).

After the establishing of the equilibrium and the definition of the constitutive equations, it is possible to write the equations of motion of the system with the Paiva et al. (2005) model. From the stress definition and the Eqs. (2) and (4), the equation of motion (1) of the structure can be rewritten as:

$$m\ddot{X} + c\dot{X} + 2A_s \frac{X}{(X^2+B^2)^{1/2}} \left\{ E \left[\frac{(X^2+B^2)^{1/2}}{L_0} + \right.\right. \\ \left.\left. -1 \right] (\alpha + E\alpha_h)(\beta_2 - \beta_1) - \kappa(T - T_0) \right\} = P(t)\,. \tag{10}$$

Considering an external periodic excitation $P(t) = P_0 \sin(\omega t)$ in the central joint, Eq. (10) may be written in nondimensional form as:

$$\begin{aligned} \dot{x}_1 &= x_2\,, \\ \dot{x}_2 &= \gamma \sin(\Omega\tau) - \bar{c}x_2 - \zeta_E \left[1 - \frac{1}{(x_1^2+b^2)^{1/2}} \right] x_1 + \\ &\quad - \Big[(\bar{\alpha} + \zeta_E \alpha_h)(\beta_2 - \beta_1) + \\ &\quad - \bar{\kappa}\zeta_\kappa(\theta - \theta_0) \Big] \frac{x_1}{(x_1^2+b^2)^{1/2}}\,, \end{aligned} \tag{11}$$

where

$$\begin{aligned} & x_1 = \frac{X}{L_0}\,, \quad b = \frac{B}{L_0}\,, \quad \theta = \frac{T}{T_M}\,, \quad \bar{\alpha} = \frac{\alpha}{E_M}\,, \\ & \zeta_E = \frac{E}{E_M}\,, \quad \zeta_\kappa = \frac{\kappa}{\kappa_M}\,, \quad \bar{\kappa} = \frac{\kappa_M T_M}{E_M}\,, \\ & \omega_0^2 = \frac{2E_M A_s}{mL_0}\,, \quad \Omega = \frac{\omega}{\omega_0}\,, \quad \bar{c} = \frac{c}{m\omega_0}\,, \\ & \gamma = \frac{P_0}{mL_0\omega_0^2}\,, \quad \dot{x}_i = \frac{\mathrm{d}x_i}{\mathrm{d}\tau} \quad \text{and} \quad \tau = \omega_0 t\,. \end{aligned} \tag{12}$$

Note that, the parameters presented in Eq. (12) are nondimensional variables and constants associated, respectively, to the system response and the SMA properties previously defined.

2.2. Constitutive model by Falk (1980)

Although the model proposed by Paiva et al. (2005) captures the general thermomechanical behavior of the SMAs, there are many simpler alternatives that provide an approximate description of the material response, but present limitations in representing hysteretic effects and the dynamic nature of phase transformations. Nevertheless, such simplified models are promising for the design of control strategies applied to this class of structures, since they offer a mathematically tractable formulation, require the adjustment of a reduced number of parameters, and involve low computational cost (Bessa et al., 2013). In this context, one of the simplest alternatives is the polynomial model that does not considers internal variables, being dependent on strain and temperature (Falk, 1980). This model considers austenite (A) and two variants of martensite ($M+, M-$) as the macroscopic phases, and it is based on a temperature dependent sixth degree polynomial free energy in terms of the uniaxial strain ε. The polynomial is chosen in such a way that its minima and maxima are associated with the stability and instability of each phase. On this basis, the SMA thermomechanical behavior is given by the following equation:

$$\sigma = a_1(T - T_M)\varepsilon - a_2\varepsilon^3 + a_3\varepsilon^5\,, \tag{13}$$

where a_1, a_2 and a_3 are related to material constants. The temperature below which the martensitic phase is stable (T_M) and the temperature above which the austenite is stable (T_A) are related to the material constants as follows:

$$T_A = T_M + \frac{1}{4}\frac{a_2^2}{a_1 a_3}\,. \tag{14}$$

From the Eqs. (1), (2) and (13), the structure dynamics with the polynomial model can be represented as follows:

$$\begin{aligned} & m\ddot{X} + c\dot{X} + \tfrac{2A_{st}}{L_0} X \Big\{ [a_1(T - T_M) - 3a_2 + 5a_3] + \\ &\quad + [-a_1(T - T_M) + a_2 - a_3] L_0 (X^2+B^2)^{-1/2} + \\ &\quad + [3a_2 - 10a_3] \tfrac{1}{L_0}(X^2+B^2)^{1/2} + \\ &\quad + [-a_2 + 10a_3] \tfrac{1}{L_0^2}(X^2+B^2) + \\ &\quad - \tfrac{5a_3}{L_0^3}(X^2+B^2)^{3/2} + \tfrac{a_3}{L_0^4}(X^2+B^2)^2 \Big\} = P(t) \end{aligned} \tag{15}$$

or in its nondimensional form,

$$\begin{aligned} \dot{x}_1 &= x_2\,, \\ \dot{x}_2 &= \gamma \sin(\Omega\tau) - \xi x_2 + x_1 \Big\{ -[\theta - 1 - 3\alpha_2 + 5\alpha_3] + \\ &\quad [\theta - 1 - \alpha_2 + \alpha_3](x_1^2+b^2)^{-1/2} + \\ &\quad - [3\alpha_2 - 10\alpha_3](x_1^2+b^2)^{1/2} + \\ &\quad [\alpha_2 - 10\alpha_3](x_1^2+b^2) + 5\alpha_3(x_1^2+b^2)^{3/2} + \\ &\quad - \alpha_3(x_1^2+b^2)^2 \Big\}\,, \end{aligned} \tag{16}$$

where ξ is a nondimensional viscous damping coefficient and α_2 and α_3 are nondimensional parameters defined as:

$$\alpha_2 = \frac{a_2}{a_1 T_M} \quad \text{and} \quad \alpha_3 = \frac{a_3}{a_1 T_M}\,. \tag{17}$$

The other parameters of Eq. (16) are defined in the same way as those presented in Eq. (12). The dissipation due to hysteretic effect on the SMA in the structure may be considered by assuming an equivalent viscous damping related to the parameter ξ.

2.3. Comparative analysis of the constitutive models

The constitutive models by Paiva et al. (2005) and Falk (1980) offer distinct approaches for simulating the thermomechanical behavior of shape memory alloys. The main advantage of the first is its capability to accurately describe a broader range of behaviors of SMAs, presenting a close agreement with experimental data. On the other hand, the polynomial model is easier to be implemented and may be preferred in applications where a just qualitative description of behavior is sufficient, and computational speed is crucial.

The simulation of the SMA thermomechanical behavior using the model by Paiva et al. (2005) is achieved through an iterative numerical procedure based on the operator split technique (Ortiz et al., 1983) and the orthogonal projection algorithm (Savi and Braga, 1993). These methods are employed to address the nonlinearities inherent in the system's formulation. The volume fraction of each phase, as described by Eqs. (5)–(7), are solved independently, defining a trial state without considering the sub-differentials of both J_π and J_χ indicator functions. If the resulting values of β_i do not comply with the internal constraints defined by the convex set π, the orthogonal projection algorithm is employed to correct the volume fraction of each phase, ensuring adherence to the imposed constraints. Fig. 2 illustrates both a typical mechanical response of an SMA at 373 K employing model by Paiva et al. (2005), as well as an approximate polynomial response derived using the polynomial model by Falk (1980). These responses employs properties specified in Tables 1 and 2.

As anticipated throughout the modeling discussion, the model by Paiva et al. (2005) properly represents the main features of the SMA behavior, including hysteresis, while the polynomial model by Falk (1980) considers just the thermomechanical equilibrium curve. On this basis, this work considers that the dynamical system is governed by

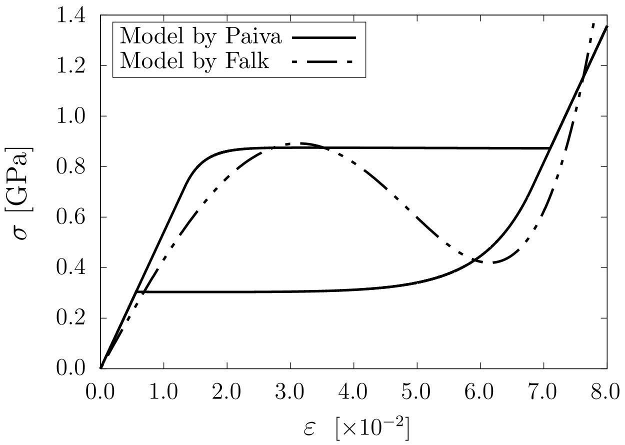

Fig. 2. Polynomial stress–strain curve matched with the hysteresis loop of the SMA at 373 K.

Table 1
SMA constitutives parameters considered in numerical simulations of the Paiva et al. (2005) model.

E_A (GPa)	E_M (GPa)	α (MPa)	α_h
54	54	150	0.052
l (MPa)	l_0 (MPa)	l_0^A (MPa)	l^A (MPa)
41.5	0.15	0.63	185
κ_A (MPaK^{-1})	κ_M (MPaK^{-1})	T_M (K)	T_A (K)
0.74	0.17	291.4	307.7
	η^L (MPa s)	η^U (MPa s)	
	10	27	

Table 2
Parameters considered in numerical simulations of the Falk (1980) model.

a_1 (MPa/K)	a_2 (MPa)	a_3 (MPa)
566.62	2.09×10^7	2.69×10^9

the model proposed by Paiva et al. (2005), which is more suitable to represent SMA thermomechanical behavior, while the controller is described by the polynomial model by Falk (1980), allowing to estimate the dynamics of the plant to be controlled.

It should be emphasized that the polynomial constitutive model is not intended to reproduce the complete thermomechanical behavior of SMAs. In particular, hysteresis loops, phase transformation paths, and temperature-dependent internal variables are not represented with the same accuracy as in more comprehensive constitutive models. Its role in the present work is to provide a simplified control-oriented representation of the plant, with low computational cost and a reduced number of parameters. This choice leads to an inherent modeling mismatch between the plant and the controller, since important nonlinear and hysteretic effects are not explicitly represented in the polynomial model. As a consequence, the controller must be able to compensate for modeling inaccuracies, unmodeled dynamics, and external disturbances. This requirement motivates the adoption of an intelligent control strategy with learning and adaptation capabilities, which is discussed in detail in the next section.

3. Control design

Intelligent control methods, such as neural network-based control, fuzzy logic control, and machine learning-based control, offer promising solutions for controlling nonlinear systems. Their main advantage lies in the ability to deal with modeling uncertainties, unmodeled dynamics, and external disturbances. Fuzzy-based approaches, for instance, can incorporate heuristic information into the controller design, whereas reinforcement learning techniques may provide adaptive data-driven policies without requiring a complete mathematical model of the plant. However, these approaches may require extensive rule tuning, large training datasets, or increased computational effort depending on the application (Mamdani, 1974; Sutton et al., 1998). In situations where the plant dynamics are sufficiently characterized and the uncertainties can be properly bounded, conventional nonlinear control techniques may be adequate. However, when the system dynamics cannot be fully represented in the controller formulation, intelligent approaches provide additional flexibility through learning and adaptation capabilities.

A powerful approach combines sliding mode control (SMC) with artificial neural networks (ANNs) (Fei and Ding, 2012; Liu et al., 2020; Su et al., 2022). SMC ensures system stability and performance by creating a sliding motion along the system state trajectory, making it robust against uncertainties. ANNs, on the other hand, are effective in approximating uncertainties in the system dynamics, rendering them well-suited for control applications with incomplete knowledge of the plant. Furthermore, ANNs provide valuable tools for addressing the challenges associated with flexible structures and manipulators (Tian and Collins, 2005; Liu et al., 2019). Their capability to model intricate nonlinearities, adapt to changing conditions, and manage uncertainties in both perception and control positions them as a vital component in advancing the capabilities of such robotic systems. Their flexibility and learning capabilities empower these systems to excel in diverse and dynamic environments.

Integrating SMC with ANNs combines the robustness of SMC and the adaptability of ANNs. Using a single hidden layer neural network, whose universal approximation property has been mathematically established in the literature (Hornik et al., 1989; Scarselli and Tsoi, 1998), allows for the compensation of uncertainties and adaptation to system changes, while simplifying the design process (Bessa et al., 2018; Dos Santos and Bessa, 2019; Lima et al., 2023). This approach significantly enhances system robustness against unexpected disturbances and parameter variations.

In order to present the SMC technique, consider a generic autonomous system described by the following ordinary differential equation:

$$x^{(n)} = f(\mathbf{x}) + g(\mathbf{x})u + p\,, \tag{18}$$

where x is the system output variable, u is the control input and p represents an external excitation. The system dynamics and the control gain are represented by the nonlinear functions f and g, respectively. The state vector of the system is given by $\mathbf{x} = [x \;\; \dot{x} \;\; \dots \;\; x^{n-1}]^\top$, where n is the order of the system.

The control problem involves driving the state vector $\mathbf{x}$ to a specific state or trajectory $\mathbf{x}_d = [x_d \;\; \dot{x}_d \;\; \dots \;\; x_d^{n-1}]^\top$, despite uncertainties in the system functions f and g. To address this problem, the SMC methodology converts the n-order tracking problem in $\mathbf{x}$ to a first-order stabilization problem in $s(\tilde{\mathbf{x}})$, where $s : \mathbb{R}^n \to \mathbb{R}$ is a switching variable called the sliding surface, and $\tilde{\mathbf{x}} = [\mathbf{x} - \mathbf{x}_d]$ represents the stabilization (or tracking) error vector. According to Slotine and Li (1991), the sliding surface is defined as:

$$s(\tilde{\mathbf{x}}) = \left(\frac{\mathrm{d}}{\mathrm{d}t} + \lambda\right)^{n-1} \tilde{x} = \boldsymbol{\Lambda}^\top \tilde{\mathbf{x}}\,, \tag{19}$$

where λ is a positive constant, and $\tilde{x}$ is the stabilization error associated with the state variable x. To ensure the stability of the system, the polynomial $\lambda^{n-1} + c_{n-1}\lambda^{n-2} + \cdots + c_2\lambda + c_1$ must be Hurwitz, with $\boldsymbol{\Lambda} = [\lambda^{n-1} \;\; c_{n-1}\lambda^{n-2} \;\; \dots \;\; c_2\lambda \;\; c_1]^\top$ and $c_i, (i = 1, 2, \dots, n-1)$ representing coefficients.

To achieve sliding mode control, the control law should ensure that the system reaches the sliding surface $s = 0$ within a finite time interval. Once the sliding phase is established, the error $\tilde{\mathbf{x}}$ converges to zero as $t \to \infty$.

When developing the control law, the following assumptions must be considered:

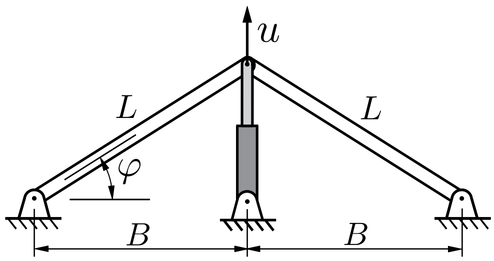

Fig. 3. Schematic illustration of an actuated von Mises truss.

Assumption 1. The state vector $\mathbf{x}$ is assumed to be available to the controller.

Assumption 2. The system dynamics f is unknown to the controller, but it is assumed to be bounded by a known function of $\mathbf{x}$, i.e., $|\hat{f} - f| \leq \mathcal{F}(\mathbf{x})$, where $\hat{f}$ is an estimate of f.

Assumption 3. The external excitation p is unknown to the controller, but it is assumed to be bounded by a known function $\mathcal{P}$, i.e., $|p| \leq \mathcal{P}$.

To ensure vibration suppression of the SMA von Mises structure, a linear actuator is used as the control action. The actuator is positioned vertically at the central joint, as shown in the Fig. 3.

There are several options for selecting an actuator to supply the control action for the structure. In this regard, it should be pointed out potential options as electro-hydraulic and electro-pneumatic actuators, as well as SMA bars. In this work, a linear actuator is of concern and the related control variable u must be taken into account in Eq. (11), which can be simply rewritten as:

$$\dot{x}_1 = x_2\,, \qquad \dot{x}_2 = p + f + u\,, \tag{20}$$

where u is the nondimensional control input, $p = \gamma \sin(\Omega\tau)$ is the nondimensional external excitation and f is the nondimensional system dynamics, which is given, based on Eq. (11), by:

$$\begin{aligned} f = & -\bar{c}x_2 - \zeta_E \left[1 - \frac{1}{(x_1^2 + b^2)^{1/2}}\right] x_1 + \\ & - \left[(\bar{\alpha} + \zeta_E \alpha_h)(\beta_2 - \beta_1) + \right. \\ & \left. - \bar{\kappa}\zeta_\kappa(\theta - \theta_0) \right] \frac{x_1}{(x_1^2 + b^2)^{1/2}}\,. \end{aligned} \tag{21}$$

The sliding surface for the SMA von Mises truss can be defined as $s = \tilde{x}_2 + \lambda\tilde{x}_1$. The control law for the system combines $u = -\hat{f} - \hat{p} + \dot{x}_{2d} - \lambda\tilde{x}_2$ with another term $-K\mathrm{sat}(s/\phi)$ to provide robustness without introducing chattering (Fuh, 2008), as follows:

$$u = -\hat{f} - \hat{p} + \dot{x}_{2d} - \lambda\tilde{x}_2 - K\mathrm{sat}(s/\phi)\,, \tag{22}$$

where $\hat{f}$ is an estimate of f, $\hat{p}$ is an estimate of p, K is positive gain, ϕ is a positive constant that represents the boundary layer thickness, given by the region $S_\phi = \left\{ \tilde{\mathbf{x}} \in \mathbb{R}^n \,\middle|\, |s(\tilde{\mathbf{x}})| \leq \phi \right\}$, and $\mathrm{sat}(s/\phi)$ is defined as:

$$\mathrm{sat}(s/\phi) = \begin{cases} \mathrm{sgn}(s/\phi) & \text{if} \quad |s/\phi| \geq 1\,, \\ s/\phi & \text{if} \quad |s/\phi| < 1\,, \end{cases} \tag{23}$$

such that $\mathrm{sng}(\cdot)$ and $\mathrm{sat}(\cdot)$ are the signal and saturation functions, respectively.

It is customary to choose a control law that satisfies the sliding condition $s\dot{s} = \vartheta|s|$, where ϑ is a strictly positive constant related to the time required to reach the sliding surface. Therefore, taking into account Assumptions 2 and 3, the robustness of the adopted smooth sliding mode controller against modeling inaccuracies and external excitation is ensured by defining K as follows:

$$K \geq \vartheta + \mathcal{F} + \mathcal{P} + |\hat{p}|. \tag{24}$$

From Eq. (16), it is possible to define the approximate dynamics of the system ($\hat{f}$), which is obtained with the model by Falk (1980), as:

$$\begin{aligned} \hat{f} = & -\xi x_2 + x_1 \, \{ -[\theta - 1 - 3\alpha_2 + 5\alpha_3] + \\ & [\theta - 1 - \alpha_2 + \alpha_3](x_1^2 + b^2)^{-1/2} + \\ & - [3\alpha_2 - 10\alpha_3](x_1^2 + b^2)^{1/2} + \\ & [\alpha_2 - 10\alpha_3](x_1^2 + b^2) + 5\alpha_3(x_1^2 + b^2)^{3/2} + \\ & - \alpha_3(x_1^2 + b^2)^2 \, \}\,. \end{aligned} \tag{25}$$

This simplified approach avoids the complexity of models that require extensive parameters and equations to estimate macroscopic phase fractions, ensuring a more manageable controller that demonstrates both robustness and intelligence.

The external excitation $\hat{p}$, that is assumed to be unknown for the controller, can be computed using various strategies. In this work, it is defined through a single hidden neural network with an online method for adjusting its weights, which makes the controller intelligent. For comparison purposes, a purely adaptive law, which represents a particular case of the intelligent scheme, is also presented to compute $\hat{p}$ in Eq. (22). On this basis, both strategies are presented, establishing the equations and pointing out the differences between them. By means of a Lyapunov-like stability analysis, the boundedness and convergence properties of the closed-loop signals with the intelligent scheme are provided. This scheme represents the controller proposed in the present work.

3.1. Intelligent scheme

Considering that a feedforward neural network with a single hidden layer can approximate continuous nonlinear functions under suitable conditions (Hornik et al., 1989; Scarselli and Tsoi, 1998), such a structure is adopted to estimate the external disturbance $\hat{p}$, as well as the neglected dynamical effects represented in the controller by $\hat{f}$. In addition, its online adaptation capability allows the controller to adjust to modeling inaccuracies and uncertainties during system operation.

With the aim of reducing the number of activation functions and the weight vector of the neural network, the sliding surface s is considered as the input of the activation functions, instead of all state variables, as presented in Fig. 4. Considering that each neuron is associated with an activation function ρ and a numerical value w, called weight, the final output $\hat{p}$ can be computed as follows:

$$\hat{p}(s) = \mathbf{w}^\top \boldsymbol{\rho}, \tag{26}$$

where $\mathbf{w} = [w_1 \;\; w_2 \;\; \dots \;\; w_n]^\top$ is the weight vector and $\boldsymbol{\rho} = [\rho_1 \;\; \rho_2 \;\; \dots \;\; \rho_n]^\top$ is the vector with the activation functions associated with the n neurons, as illustrated in Fig. 4(a). In the present work, Gaussian activation functions and centers defined in accordance with the boundary layer width (ϕ) are adopted, as shown in Fig. 4(b). The weight vector $\mathbf{w}$ is updated according to the following equation:

$$\dot{\mathbf{w}} = \psi \boldsymbol{\rho} s\,, \tag{27}$$

where ψ represents the learning rate of the neural network weights.

Finally, for a better understanding of the intelligent control law described by Eq. (22), a schematic diagram is presented in Fig. 5. The priori knowledge is provided by $\hat{f}$, as described in Eq. (25). Eq. (26), on the other hand, offers a posteriori knowledge, learning from the system's interaction with its environment. Eq. (27) enables real-time adjustments to the neural network's weight vector, taking into account factors such as the adaptation rate ψ, sliding surface s, and activation functions $\boldsymbol{\rho}$. The real-time nature of the proposed adaptation law encourages the use of locally supported activation functions to guarantee the preservation of learned experiences.

Since an intelligent controller must be capable of prediction, adaptation, learning, and robustness to emulate fundamental aspects of intelligence (Bessa et al., 2018), the controller proposed in this work can be regarded as intelligent. These characteristics allow it to anticipate actions, adjust to changes that occur in the environment, learn from interactions, and maintain stability under varied conditions.

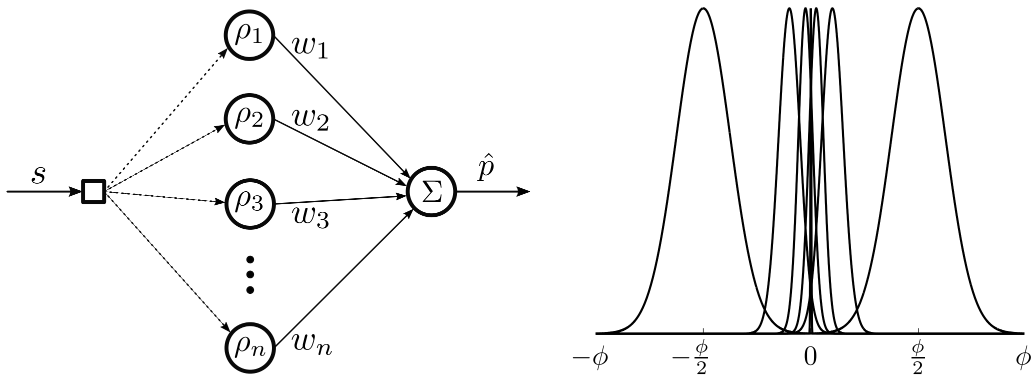

(a) Single hidden layer network. (b) Gaussian activation functions.

Fig. 4. Neural network and its activation functions considered in the present work.

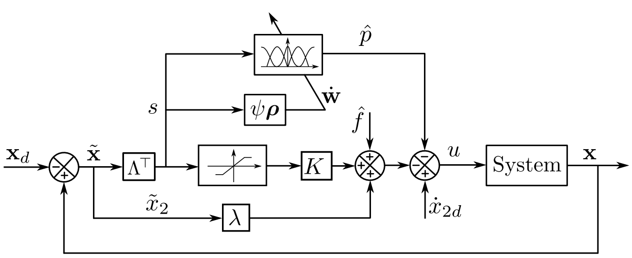

Fig. 5. Schematic diagram of the intelligent control.

3.2. Purely adaptive law

It is important to note that the attributes presented in the intelligent scheme can be used to distinguish between a broad range of control schemes. Controllers that operate on a purely adaptive basis are deficient in their capacity to learn from interactions with the environment, requiring constant adaptation, even to situations that have been previously experienced. Hence, it can be deduced that controllers exclusively dependent on purely adaptive strategies fail to satisfy the essential characteristics attributed to intelligence.

Some controllers that incorporate soft computing techniques might be regarded as intelligent within a broad framework. Artificial neural networks, which utilize supervised offline training, and fuzzy methods built on heuristic principles, are extensively used for control purposes. Nevertheless, a system governed by such a controller would not be able to adapt in the face of new experiences, neither would it perform online learning by interacting with the environment. Therefore, in a strict sense, this control system would not be capable of manifesting intelligent behavior.

It is important to highlight that the ability to emulate intelligence does not guarantee better control performance. There are situations where robust methods or purely adaptive ones can effectively deal with plants subject to structured uncertainties.

A purely adaptive law can be obtained based on Eq. (26) and (27). This modification involves the adoption of a single neuron in the hidden layer with an activation function $\rho = 1$ for all s. Consequently, the output $\hat{p}$ from Eq. (22) can be calculated as follows:

$$\dot{\hat{p}} = \psi s, \tag{28}$$

where ψ is a strictly positive constant related to the adaptation rate of the purely adaptive law.

3.3. Stability analysis

At this point, a Lyapunov-like stability analysis is conducted to investigate the boundedness and convergence properties of the intelligent control. Considering $\tilde{\mathbf{w}} = \mathbf{w} - \mathbf{w}_*$ as the deviation in relation to the optimal parameter vector $\mathbf{w}_*$ associated with the optimal estimate $\hat{p}_*(s)$, then a positive-definite function V can be defined as:

$$V = \frac{1}{2}s^2 + \frac{1}{2\psi}\tilde{\mathbf{w}}^\top\tilde{\mathbf{w}}, \tag{29}$$

where ψ is a positive constant. Thus, the time derivative of V is given by:

$$\begin{aligned}\dot{V} &= s\dot{s} + \psi^{-1}\tilde{\mathbf{w}}^\top\dot{\mathbf{w}}\\ &= (\dot{x}_2 - \dot{x}_{2d} + \lambda\tilde{x}_2)s + \psi^{-1}\tilde{\mathbf{w}}^\top\dot{\mathbf{w}}\\ &= (p + f + u - \dot{x}_{2d} + \lambda\tilde{x}_2)s + \psi^{-1}\tilde{\mathbf{w}}^\top\dot{\mathbf{w}}\,.\end{aligned} \tag{30}$$

Considering the approximation error as $\epsilon = \mathbf{w}_*^\top\boldsymbol{\rho} - p$, Assumption 2, and applying the control law (22) and Eq. (26) in Eq. (30), $\dot{V}$ becomes:

$$\begin{aligned}\dot{V} &= -\left[\,(\hat{p} + \epsilon - \mathbf{w}_*^\top\rho) + \mathcal{F} + K\mathrm{sat}(s/\phi)\,\right] s +\\ &\quad \psi^{-1}\tilde{\mathbf{w}}^\top\dot{\mathbf{w}}\\ &= -\left[\,\tilde{\mathbf{w}}^\top\rho + \mathcal{F} + K\mathrm{sat}(s/\phi) + \epsilon\,\right] s + \psi^{-1}\tilde{\mathbf{w}}^\top\dot{\mathbf{w}}\\ &= -\left[\,\mathcal{F} + K\mathrm{sat}(s/\phi) + \epsilon\,\right] s + \psi^{-1}\tilde{\mathbf{w}}^\top(\dot{\mathbf{w}} - \psi\rho s)\,.\end{aligned} \tag{31}$$

Therefore, by updating $\mathbf{w}$ according to Eq. (27), the time derivative of the Lyapunov function, $\dot{V}$, is reduced for:

$$\dot{V} = -\left[\,\mathcal{F} + K\mathrm{sat}(s/\phi) + \epsilon\,\right] s. \tag{32}$$

Now, the projection algorithm is introduced, being defined by the following equation:

$$\dot{\mathbf{w}} = \begin{cases} \psi\boldsymbol{\rho}s, & \begin{array}{l}\text{if } \|\mathbf{w}\|_2 < \Gamma \text{ or}\\ \text{if } \|\mathbf{w}\|_2 = \Gamma \text{ and } \psi s\mathbf{w}^\top\boldsymbol{\rho} \le 0,\end{array}\\ \left(I - \dfrac{\mathbf{w}\mathbf{w}^\top}{\mathbf{w}^\top\mathbf{w}}\right), & \text{otherwise,}\end{cases} \tag{33}$$

where Γ represents the desired upper bound for $\|\mathbf{w}\|_2$.

The projection algorithm plays a pivotal role in ensuring the stability and reliability of the control system by enforcing constraints on states and control inputs. It guarantees that the neural network's weights adhere to predefined bounds, thereby maintaining system stability and robustness. This algorithm can prevent variables from exceeding safe limits, ultimately enhancing the system's resilience to disturbances and uncertainties. Moreover, it simplifies the control design process and is essential for real-world applications where physical limits must be respected.

Outside the boundary layer, i.e., when $|s/\phi| \ge 1$, the time derivative of V becomes:

$$\dot{V} = -\left[\,\mathcal{F} + K\mathrm{sgn}(s) + \epsilon\,\right] s. \tag{34}$$

Furthermore, considering Assumptions 2 and 3, defining K according to Eq. (24) and verifying that $|\epsilon| = |\hat{p}_* - p| \le |\hat{p} - p| \le |\hat{p}| + \mathcal{P}$, one obtains:

$$\dot{V} \le -\vartheta|s|\,. \tag{35}$$

Integrating both sides, Eq. (35) shows that:

$$\lim_{t\to\infty}\int_0^t \vartheta|s|dv \leq \lim_{t\to\infty}\left[\, V(0)-V(t)\,\right] \leq V(0) < \infty\,. \tag{36}$$

Since the absolute value function is uniformly continuous function of time, it follows from Barbalat's lemma (Khalil and Grizzle, 2002) that the intelligent control law ensures the convergence of the tracking error to the boundary layer.

Inside the boundary layer, i.e., when $|s/\phi| < 1$, the convergence of the tracking error can be investigated as follows:

$$-\phi \leq s \leq \phi\,. \tag{37}$$

Multiplying by $e^{\lambda t}$, Eq. (37) becomes:

$$-\phi e^{\lambda t} \leq \frac{d}{dt}\left(\tilde{x}_1 e^{\lambda t}\right) \leq \phi e^{\lambda t}\,. \tag{38}$$

Integrating Eq. (38) from 0 to t, one gets:

$$\begin{aligned}
&-\frac{\phi}{\lambda}\left(e^{\lambda t}-1\right) \leq \tilde{x}_1(t)e^{\lambda t} - \tilde{x}_1(0) \leq \frac{\phi}{\lambda}\left(e^{\lambda t}-1\right)\\
&\quad -\frac{\phi}{\lambda}\left(1-\frac{1}{e^{\lambda t}}\right) + \frac{\tilde{x}_1(0)}{e^{\lambda t}} \leq \tilde{x}_1(t)\\
&\quad \tilde{x}_1(t) \leq \frac{\phi}{\lambda}\left(1-\frac{1}{e^{\lambda t}}\right) + \frac{\tilde{x}_1(0)}{e^{\lambda t}}\,.
\end{aligned} \tag{39}$$

When t tends to infinity, the error band is obtained:

$$\begin{aligned}
&\lim_{t\to\infty}\left[-\frac{\phi}{\lambda}\left(1-\frac{1}{e^{\lambda t}}\right) + \frac{\tilde{x}_1(0)}{e^{\lambda t}}\right] \leq \tilde{x}_1(t)\\
&\lim_{t\to\infty}\left[\frac{\phi}{\lambda}\left(1-\frac{1}{e^{\lambda t}}\right) + \frac{\tilde{x}_1(0)}{e^{\lambda t}}\right] \geq \tilde{x}_1(t)\\
&\quad -\frac{\phi}{\lambda} \leq \tilde{x}_1(t) \leq \frac{\phi}{\lambda}\,.
\end{aligned} \tag{40}$$

With the tracking error range (40) and Eq. (38), it is possible to determine the range of the derivative of error $\tilde{x}_1$, as follows:

$$-2\phi \leq \tilde{x}_2(t) \leq 2\phi\,. \tag{41}$$

Therefore, the intelligent control law defined by (22), (26), and (27) ensures the exponential convergence of the error to the closed region $\mathcal{X} = \left\{\, \tilde{\mathbf{x}} \in \mathbb{R}^2 \,\middle|\, |\tilde{x}_i| \leq i\lambda^{i-2}\phi, i = 1,2 \,\right\}$.

4. Numerical simulations

The dynamical behavior of the SMA von Mises truss and the performance of the proposed control scheme are now studied through numerical simulations. Time integration is performed by using the classical fourth-order Runge–Kutta method and the material properties specified in tables 1 and 2 are consistently applied in all simulations, representing typical SMA properties.

4.1. Uncontrolled dynamics

In order to achieve a global comprehension of the system dynamics, bifurcation diagrams are of concern by sampling the central joint's displacement (x_1) under varying parameters. A high temperature (T = 373 K) behavior is adopted where the austenitic phase is stable at stress-free state, presenting a pseudoelastic behavior. Two scenarios are examined: one with a fixed nondimensional frequency ($\Omega = 0.475$) and varying nondimensional amplitude (γ) of external excitation, and another with a fixed $\gamma = 0.01$ and varying load frequency (Ω). Time steps are chosen as $\Delta\tau = \pi/1000\Omega$. Parameters follow Table 1 with b = 0.894, $\bar{c} = 0.0$, and an initial condition $\mathbf{x}(0) = [0.447 \;\; 0.0]^{\top}$, representing a stable equilibrium point.

Bifurcation diagrams in Fig. 6 reveal regions associated with chaotic and periodic motions, varying with frequency and amplitude. The analysis covers a range of forcing frequency and amplitude, yielding periodic, quasi-periodic, and chaotic behaviors, as illustrated in Figs. 6(a) and 6(b).

Fig. 7 presents a detailed view of the dynamic behavior of the shape memory von Mises structure. Notably, it exhibits a chaotic-like motion, akin to the typical strange attractors depicted in Figs. 7(b) and 7(d). In Fig. 7(a), the system's response is confined to the positive phase space, exclusively visiting positive equilibrium points. However, introducing a load frequency of $\Omega = 0.3347$ leads to a different chaotic motion. Under this condition, the system traverses the entire phase space, exhibiting both chaotic behavior and the snap-through phenomenon, illustrated in Fig. 7(c).

A comprehensive analysis of the chaotic response of the SMA von Mises structure, employing the same model as in this study, is provided by Savi and Nogueira (2010). It is noteworthy that the results derived from the bifurcation diagrams and the observed chaotic motion align with their findings.

4.2. Controlled dynamics

The performance of the intelligent controller is now under investigation. Sampling rates of $200\Omega/\pi$ are of concern for the control system, while $1000\Omega/\pi$ is employed for the dynamical model. To provide prior knowledge to the intelligent control system, the polynomial constitutive model is employed to describe the SMA behavior of the structural bars. In contrast, the constitutive model by Paiva et al. (2005) is used exclusively to represent the plant dynamics in the numerical simulations, i.e., the system to be controlled.

This separation between the plant model and the control-oriented model highlights the capability of the adopted intelligent control scheme to cope with strong nonlinearities, uncertain parameters, unmodeled dynamics and external disturbances.

The constants a_1, a_2, and a_3 are defined in Table 2. Concerning the estimation of the system dynamics, the hysteresis effect in Eq. (25) is assumed to be unknown. Consequently, the neural network compensates for the dissipative term ξx_2 of the polynomial constitutive model.

The following parameters are assumed for the intelligent controller: $\mathcal{F} = 0.01$, $\mathcal{P} = 0.02$, $\vartheta = 0.02$, $\phi = 0.05$ and $\lambda = 0.8$. For the neural network, seven neurons with Gaussian activation functions in the hidden layer are assumed. The centers and widths of these Gaussian functions are determined based on the boundary layer width, as $\rho_c = \{-\phi; -\phi/10; -\phi/40; 0.0; \phi/40; \phi/10; \phi\}$ and $\rho_w = \{-\phi/10; -\phi/20; -\phi/30; \phi/500; \phi/30; \phi/20; \;\phi/10\}$, respectively. The weight vector is initialized as $\mathbf{w} = \mathbf{0}$ and updated at each iteration step using Eq. (27), with an adaptation rate of $\psi = 0.5$.

The use of seven Gaussian neurons is adopted as a compromise between approximation capability and computational simplicity. Since the sliding surface is the only input of the neural network, a small number of neurons is sufficient to cover the boundary layer region without increasing the computational burden. The centers are distributed around the origin, with higher concentration near the sliding surface, where accurate approximation is more relevant for stabilization. The widths are selected according to the boundary layer thickness in order to ensure overlap between neighboring activation functions and smooth approximation of the unknown dynamics and external disturbances.

In order to demonstrate that the adopted controller can deal with both modeling inaccuracies and external disturbances, the periodic excitation is treated as an unknown external stimulus. Under this assumption, $\gamma\sin(\Omega\tau)$ is not taken into account in the control law Eq. (22). According to Eq. (26), $\hat{p}$ is estimated using a single hidden layer neural network that learns in real-time during interactions with the system, providing posterior knowledge about the structure's dynamics. This approach aims to significantly reduce the vibration level of the structure while also preventing the undesired snap-through behavior. The structure presents initial condition $\mathbf{x}(0) = [0.447 \;\; 0.0]^{\top}$, matching the stabilization point $\mathbf{x}_d = [0.447 \;\; 0.0]^{\top}$, in line with the nominal

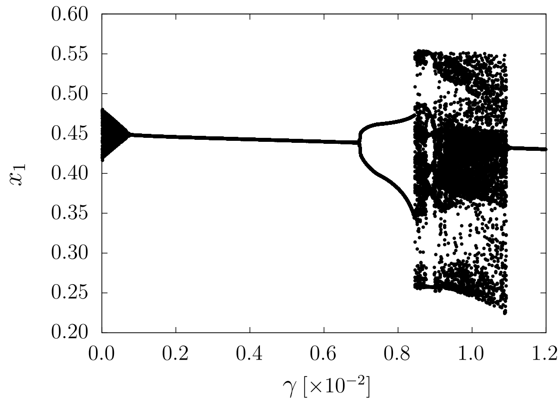

(a) Varying γ with $\Omega = 0.475$.

(b) Varying Ω with $\gamma = 0.01$.

Fig. 6. Bifurcation diagrams of the SMA von Mises truss.

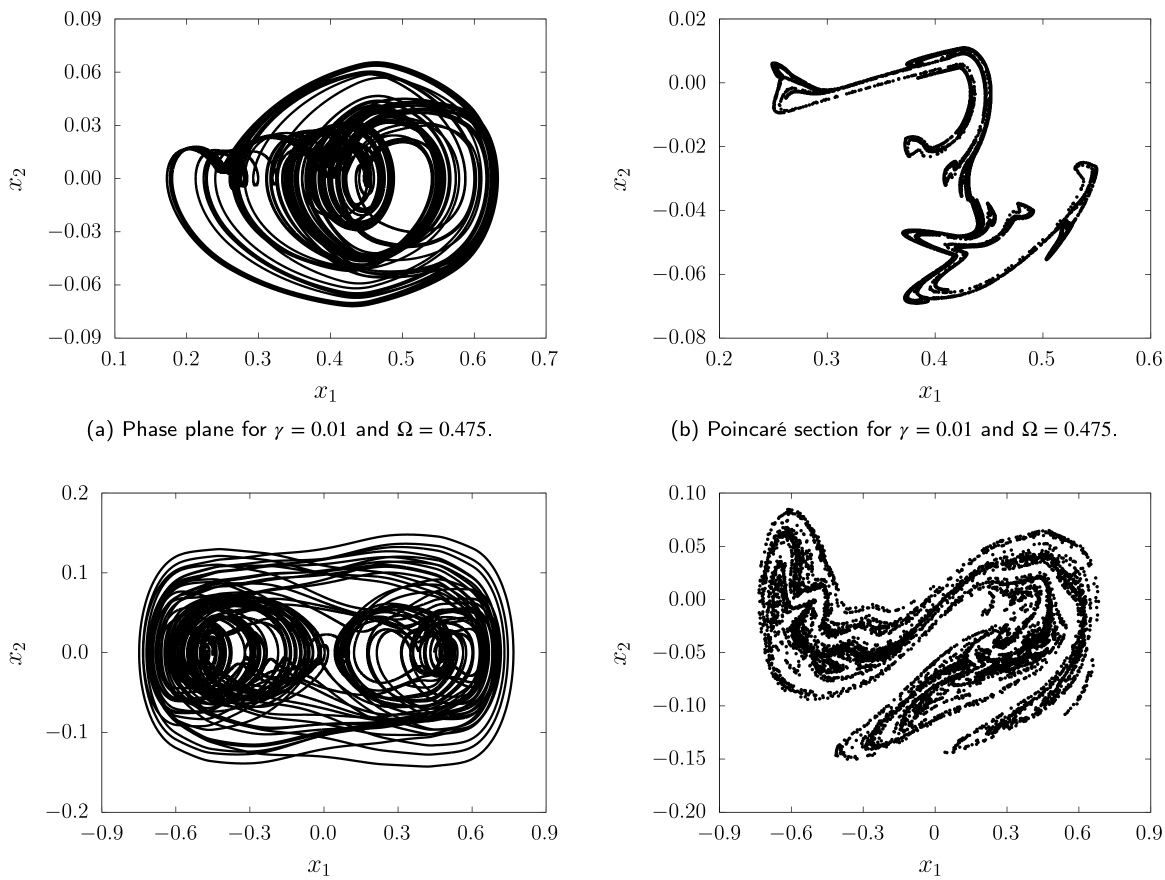

(a) Phase plane for $\gamma = 0.01$ and $\Omega = 0.475$.

(b) Poincaré section for $\gamma = 0.01$ and $\Omega = 0.475$.

(c) Phase plane for $\gamma = 0.01$ and $\Omega = 0.3347$.

(d) Poincaré section for $\gamma = 0.01$ and $\Omega = 0.3347$.

Fig. 7. Chaotic response of the SMA von Mises truss.

values of the structure. Fig. 8 shows that, with the implementation of intelligent control, the chaotic behavior characterized by large amplitudes in the uncontrolled response is replaced by a regular motion with small amplitudes around the equilibrium point $\mathbf{x}_d$. This transition occurs when the controller is activated at $\tau = 400$.

From the control performance presented in Fig. 8, the robustness of the proposed scheme can be observed. Even in the presence of unknown disturbances and the uncertain dynamical model used as prior knowledge, the intelligent scheme achieves the desired stabilization with small amplitudes. This underscores the fact that systems with strong nonlinearities and complex behaviors, such as the SMA von Mises structure, can be effectively controlled using simple constitutive models. This effectiveness is especially notable when the controller leverages essential characteristics of human intelligence, as demonstrated here.

The control performance is directly influenced by the SMA constitutive parameters, since temperature-dependent phase transformations, hysteresis, and energy dissipation modify the effective stiffness and damping of the structure. It is important to note that two different constitutive models are employed in this study. The plant dynamics used in the numerical simulations are represented by the more realistic SMA model proposed by Paiva et al. (2005), which incorporates

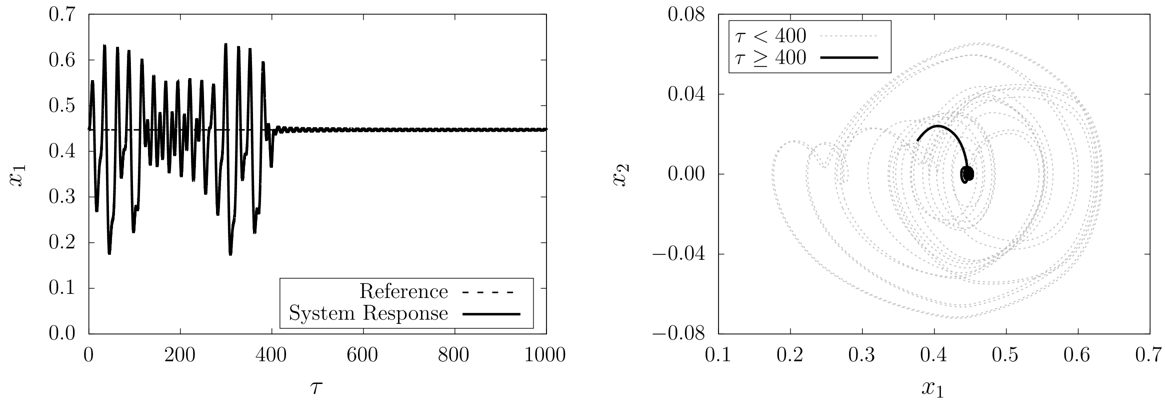

(a) Time series with $\gamma = 0.01$ and $\Omega = 0.475$.

(b) Phase plane with $\gamma = 0.01$ and $\Omega = 0.475$.

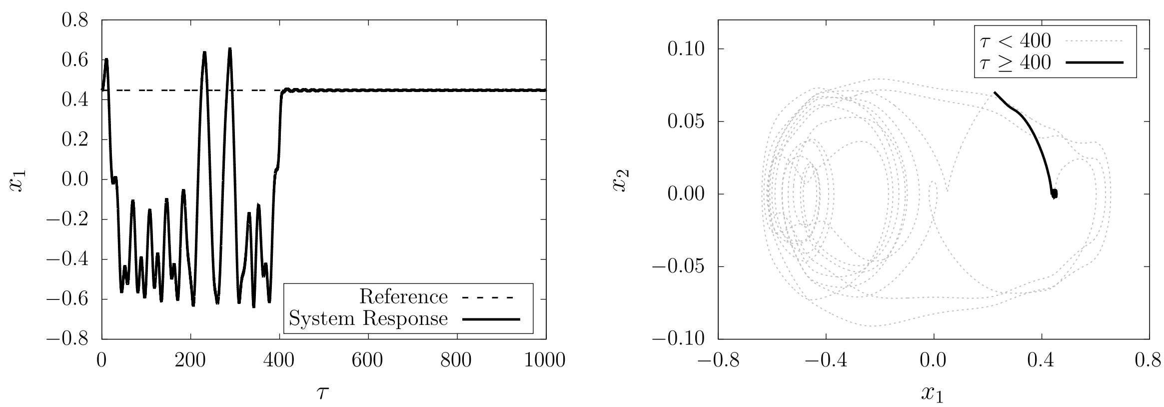

(c) Time series with $\gamma = 0.01$ and $\Omega = 0.3347$.

(d) Phase plane with $\gamma = 0.01$ and $\Omega = 0.3347$.

Fig. 8. System response when the intelligent controller is activated.

thermomechanical coupling and hysteretic behavior. In contrast, the controller is designed using the simplified polynomial constitutive model proposed by Falk (1980), which is selected due to its suitability for control-oriented applications and reduced computational complexity.

Consequently, the controller is intentionally designed under model mismatch conditions, since the simplified Falk model (Falk, 1980) does not explicitly capture several nonlinear phenomena represented by the Paiva et al. model (Paiva et al., 2005). Variations in temperature-dependent parameters, hysteresis characteristics, and phase transformation properties may further increase this mismatch. Even under these conditions, the proposed intelligent sliding mode controller maintains satisfactory stabilization performance because the neural network approximates the neglected dynamics online, while the sliding mode term provides robustness against residual uncertainties and modeling errors.

The learning capability of the intelligent scheme should be highlighted. In this regard, it is important to establish a comparison between the intelligent sliding mode controller (ISMC) and the adaptive sliding mode controller (ASMC), which describe the purely adaptive approach. By conducting a comparative analysis of the stabilization errors illustrated in Fig. 9, it is noticeable a decrease in controller accuracy when using an adaptive approximation compared to an intelligent one. Table 3 presents the Mean Square Error (MSE) and Root Mean Square Error ($RMSE$) values of the stabilization errors shown in Figs. 9(a) and 9(c).

Hence, the intelligent controller is associated with a 96.73% reduction in mean square error for the first scenario and an 83.12% reduction for the second. In addition, the proposed strategy achieves reductions of 81.93% and 41.08% in the root mean squared error for the first and second scenarios, respectively. These results reinforce the effectiveness of the intelligent control strategy, since reductions are observed in both

Table 3
Mean square error and root mean square error of the stabilization errors.

Scenario	$\gamma = 0.01; \Omega = 0.475$	$\gamma = 0.01; \Omega = 0.3347$
MSE_{ISMC}	1.307×10^{-5}	11.395×10^{-5}
MSE_{ASMC}	40.006×10^{-5}	67.515×10^{-5}
$RMSE_{ISMC}$	3.615×10^{-3}	10.675×10^{-3}
$RMSE_{ASMC}$	20.001×10^{-3}	25.984×10^{-3}

the quadratic error energy measured by the MSE and the overall error amplitude represented by the $RMSE$. This suggests that an intelligent controller presents a better performance than a purely adaptive scheme in situations requiring high-precision control. Moreover, complex structures frequently missing well-defined mathematical models, making the intelligent controller the preferred option. The superior performance of ISMC compared to ASMC is further illustrated in the phase portraits in Figs. 9(b) and 9(d). While the ASMC leads the system to limit cycles, the ISMC drives it toward errors that approach zero. Both schemes guarantee the exponential convergence of the error toward the closed region (CR) $\mathcal{X}$, defined as $\mathcal{X} = \left\{ \tilde{\mathbf{x}} \in \mathbb{R}^2 \,\middle|\, |\tilde{x}_i| \leq i\lambda^{i-2}\phi, i = 1, 2 \right\}$, as outlined by Eqs. (40) and (41).

Fig. 10 presents the control efforts of the two analyzed scenarios showing that the instant when both controllers are turned on, marked by the rapid growth of their efforts while maintaining smooth control actions. It is noteworthy that despite ISMC having significantly smaller stabilization errors compared to ASMC, the control efforts are practically identical.

Through a comparative analysis of the absolute mean effort ($|\bar{u}|$), it is obtained $|\bar{u}|_{ISMC} = 6.450\times10^{-3}$ and $|\bar{u}|_{ASMC} = 6.448\times10^{-3}$ for $\gamma = 0.01$ and $\Omega = 0.475$, which corresponds to an increase of only 0.031% in the

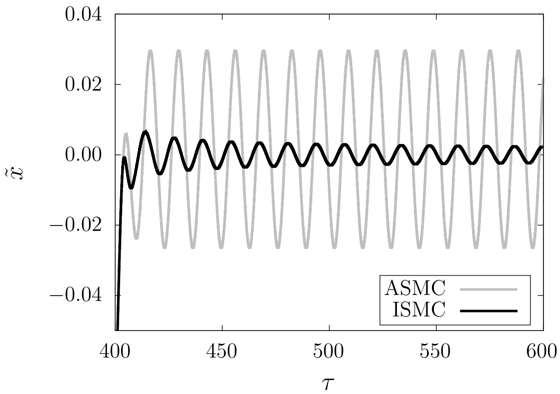

(a) Stabilization error for $\gamma = 0.01$ and $\Omega = 0.475$.

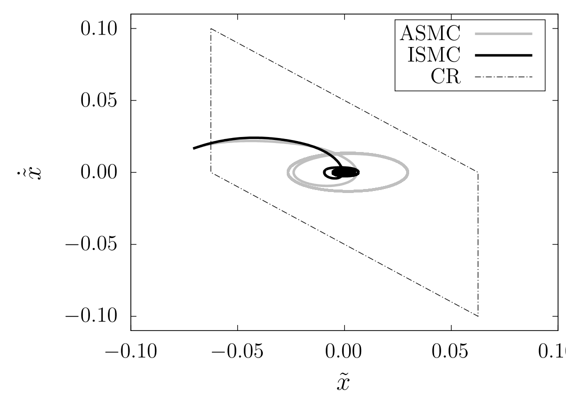

(b) Error phase plane for $\gamma = 0.01$ and $\Omega = 0.475$.

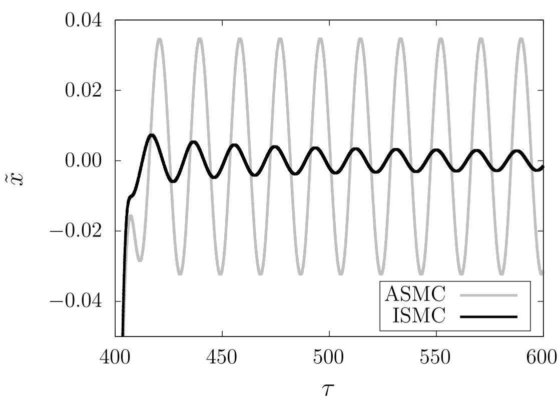

(c) Stabilization error for $\gamma = 0.01$ and $\Omega = 0.3347$.

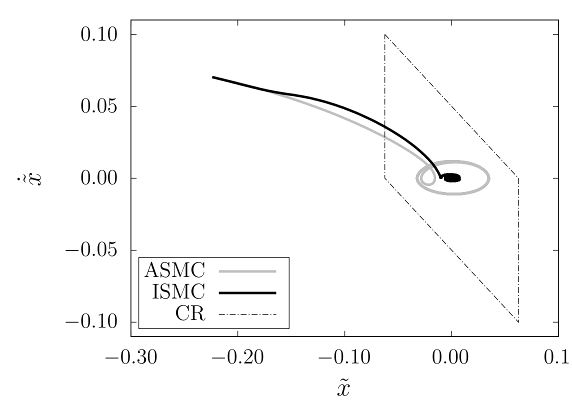

(d) Error phase plane for $\gamma = 0.01$ and $\Omega = 0.3347$.

Fig. 9. Comparative analysis of intelligent and adaptive sliding mode control.

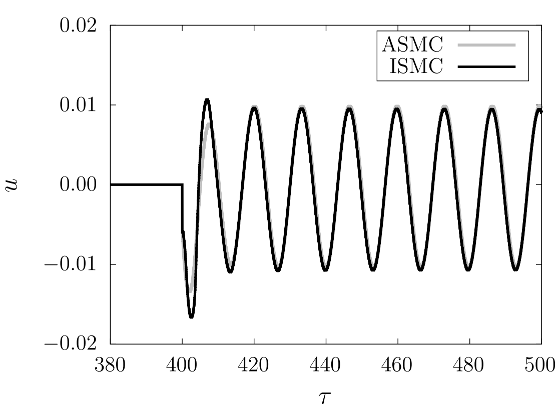

(a) Control effort for $\gamma = 0.01$ and $\Omega = 0.475$.

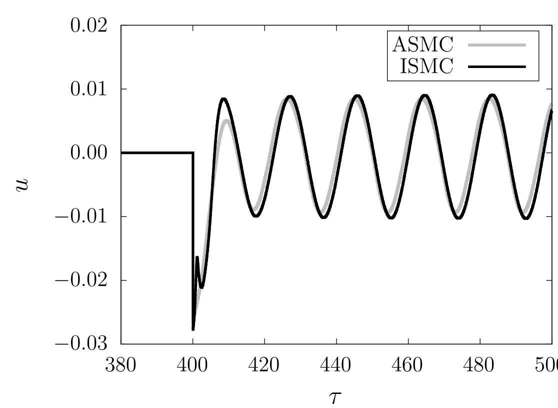

(b) Control effort for $\gamma = 0.01$ and $\Omega = 0.3347$.

Fig. 10. Comparison of control efforts with adaptive and intelligent approaches.

control effort when the ISMC is adopted, and $|\bar{u}|_{ISMC} = 6.118\times10^{-3}$ and $|\bar{u}|_{ASMC} = 5.734\times10^{-3}$ for $\gamma = 0.01$ and $\Omega = 0.3347$, which is related to an increase of only 6.7% in the control effort when the ISMC is considered.

5. Concluding remarks

In this paper, an intelligent control approach is explored based on the sliding mode technique with an online learning neural network for vibration suppression in a shape memory von Mises structure. This system is a prototype smart structure that serves as a valuable model for investigating the stability of shape memory alloy structures. The thermomechanical behavior of the structural elements employs a constitutive model that matches experimental data, alongside a simplified polynomial constitutive equation for the controller design. This polynomial model serves as prior knowledge about the plant, later refined by the neural network.

The study demonstrates the conception of an intelligent control system through the use of artificial neural networks. This system enhances adaptability and learning in control mechanisms. Unlike purely adaptive controls that cannot learn from past interactions, this system stands out by adding learning capabilities. Due to its online learning capability during interactions, the intelligent controller exhibits essential features of natural intelligence, including robustness, prediction, adaptation, and learning.

The proposed controller makes a significant contribution by enabling the control of structures and systems with complex behaviors, which often lack easily formulated analytical approaches. As demonstrated by numerical simulations, integrating a single hidden layer neural network into the boundary layer of a smooth sliding mode controller greatly enhances system stabilization in the desired state.

Remarkably, the intelligent scheme achieves significantly improved stabilization performance with nearly the same control effort compared to a purely adaptive approach. This intelligent controller effectively mitigates undesirable responses such as snap-through behavior and chaotic motion.

Although the present investigation is restricted to numerical simulations, the adopted framework provides a consistent basis for future experimental validation. Experimental investigations available in the literature have already demonstrated good agreement between theoretical predictions and experimental measurements in nonlinear SMA dynamical systems, even in the presence of hysteretic and temperature-dependent effects (Enemark et al., 2014; Sitnikova et al., 2012). Future work will focus on implementing the proposed control strategy in an experimental SMA structure, allowing the assessment of practical issues such as sensor noise, actuator limitations, temperature control, and real-time computational requirements.

CRediT authorship contribution statement

Philippe Eduardo de Medeiros: Writing – original draft, Visualization, Software, Methodology, Investigation, Data curation, Conceptualization. **Marcelo Amorim Savi:** Writing – review & editing, Supervision, Software, Resources, Project administration, Methodology, Funding acquisition, Formal analysis, Conceptualization. **Wallace Moreira Bessa:** Writing – review & editing, Supervision, Software, Resources, Project administration, Methodology, Funding acquisition, Formal analysis, Conceptualization.

Declaration of competing interest

The authors declare that they have no known competing financial interests or personal relationships that could have appeared to influence the work reported in this paper.

Acknowledgments

The authors would like to acknowledge the support of the Brazilian Research Agencies CNPq (Conselho Nacional de Desenvolvimento Científico e Tecnológico), CAPES (Coordenação de Aperfeiçoamento de Pessoal de Nível Superior), and FAPERJ (Fundação Carlos Chagas Filho de Amparo à Pesquisa do Estado do Rio de Janeiro), and through the INCT-EIE (National Institute of Science and Technology - Smart Structures in Engineering), and FAPEMIG (Fundação de Amparo à Pesquisa do Estado de Minas Gerais). The support of the AFOSR (Air Force Office of Scientific Research) (FA9550-23-4301-0527) is also acknowledged.

In addition, this work was supported by the Research Council of Finland under the Digital Waters (DIWA) Flagship (decision no. 359247).

Data availability

Data will be made available on request.

References

AbuZaiter, A., Nafea, M., Ali, M.S.M., 2016. Development of a shape-memory-alloy micromanipulator based on integrated bimorph microactuators. Mechatronics 38, 16–28. http://dx.doi.org/10.1016/j.mechatronics.2016.05.009.

Alves, M.T.S., Steffen, V., Steffen, V., dos Santos, M.C., Savi, M.A., Enemark, S., Santos, I., 2018. Vibration control of a flexible rotor suspended by shape memory alloy wires. J. Intell. Mater. Syst. Struct. http://dx.doi.org/10.1177/1045389x18758179.

Attanasi, G., Auricchio, F., 2011. Innovative superelastic isolation device. J. Earthq. Eng. 15, 72–89. http://dx.doi.org/10.1080/13632469.2011.562406.

Auricchio, F., Boatti, E., Conti, M., Marconi, S., 2021. Sma biomedical applications. In: Shape Memory Alloy Engineering. Elsevier, pp. 627–658. http://dx.doi.org/10.1016/B978-0-12-819264-1.00019-4.

Bazant, Z.P., Cedolin, L., 2010. Stability of Structures. World Scientific Publishing Co. Pte. Ltd..

Bessa, W.M., Brinkmann, G., Duecker, D.A., Kreuzer, E., Solowjow, E., 2018. A biologically inspired framework for the intelligent control of mechatronic systems and its application to a micro diving agent. Math. Probl. Eng. 2018, 1–16. http://dx.doi.org/10.1155/2018/9648126.

Bessa, W., de Paula, A.S., Savi, M., 2013. Adaptive fuzzy sliding mode control of smart structures. Eur. Phys. J. Spec. Top. 222, 1541–1551. http://dx.doi.org/10.1140/epjst/e2013-01943-7.

Brotzu, A., Di Cocco, V., Iacoviello, F., Natali, S., Vendittozzi, C., 2021. Standards for shape memory alloy applications. In: Shape Memory Alloy Engineering. Elsevier, pp. 77–111. http://dx.doi.org/10.1016/B978-0-12-819264-1.00003-0.

Chaudhari, R., Vora, J.J., Parikh, D., 2021. A review on applications of nitinol shape memory alloy. Recent. Adv. Mech. Infrastruct.: Proc. ICRAM 2020 123–132. http://dx.doi.org/10.1007/978-981-33-4176-0_10.

Chi, Y., Li, Y., Zhao, Y., Hong, Y., Tang, Y., Yin, J., 2022. Bistable and multistable actuators for soft robots: Structures, materials, and functionalities. Adv. Mater. 34, 2110384. http://dx.doi.org/10.1002/adma.202110384.

Cisse, C., Zaki, W., Zineb, T.B., 2016. A review of constitutive models and modeling techniques for shape memory alloys. Int. J. Plast. 76, 244–284. http://dx.doi.org/10.1016/j.ijplas.2015.08.006.

Copaci, D.S., Blanco, D., Martin-Clemente, A., Moreno, L., 2020. Flexible shape memory alloy actuators for soft robotics: Modelling and control. Int. J. Adv. Robot. Syst. 17, 1729881419886747. http://dx.doi.org/10.1177/1729881419886747.

Costa, D.D., Savi, M.A., de Paula, A.S., Bernardini, D., 2019. Chaos control of a shape memory alloy structure using thermal constrained actuation. Int. J. Non-Linear Mech. http://dx.doi.org/10.1016/j.ijnonlinmec.2019.02.006.

De Paula, A.S., dos Santos, M.V., Savi, M.A., Bessa, W.M., 2014. Controlling a shape memory alloy two-bar truss using delayed feedback method. Int. J. Struct. Stab. Dyn. 14, 1440032. http://dx.doi.org/10.1142/S021945541440032X.

Dos Santos, J., Bessa, W., 2019. Intelligent control for accurate position tracking of electrohydraulic actuators. Electron. Lett. 55, 78–80. http://dx.doi.org/10.1049/el.2018.7218.

Enemark, S., A Savi, M., F Santos, I., 2014. Nonlinear dynamics of a pseudoelastic shape memory alloy system—theory and experiment. Smart Mater. Struct. 23, 085018. http://dx.doi.org/10.1088/0964-1726/23/8/085018, URL https://doi.org/10.1088/0964-1726/23/8/085018.

Exarchos, D.A., Dalla, P.T., Tragazikis, I.K., Dassios, K.G., Zafeiropoulos, N.E., Karabela, M.M., De Crescenzo, C., Karatza, D., Musmarra, D., Chianese, S., et al., 2018. Development and characterization of high performance shape memory alloy coatings for structural aerospace applications. Materials 11, 832. http://dx.doi.org/10.3390/ma11050832.

Falk, F., 1980. Model free energy, mechanics, and thermodynamics of shape memory alloys. Acta Metall. 28, 1773–1780. http://dx.doi.org/10.1016/0001-6160(80)90030-9.

Falope, F.O., Pelliciari, M., Lanzoni, L., Tarantino, A.M., 2021. Snap-through and eulerian buckling of the bi-stable von mises truss in nonlinear elasticity: A theoretical, numerical and experimental investigation. Int. J. Non-Linear Mech. 134, 103739. http://dx.doi.org/10.1016/j.ijnonlinmec.2021.103739.

Fei, J., Ding, H., 2012. Adaptive sliding mode control of dynamic system using rbf neural network. Nonlinear Dynam. 70, 1563–1573. http://dx.doi.org/10.1007/s11071-012-0556-2.

Fuh, C.C., 2008. Variable-thickness boundary layers for sliding mode control. J. Mar. Sci. Technol. 16, 288–294. http://dx.doi.org/10.51400/2709-6998.2014.

Gantz, F., Stroud, H., Fuller, J.C., Adams, K., Caltagirone, P.E., Ozcan, H., Karaman, I., Hartl, D.J., Stebner, A.P., Trehern, W., et al., 2022. Aerospace, energy recovery, and medical applications: Shape memory alloy case studies for casmart 3rd student design challenge. Shape Mem. Superelasticity 8, 150–167. http://dx.doi.org/10.1007/s40830-022-00368-z.

Hornik, K., Stinchcombe, M., White, H., 1989. Multilayer feedforward networks are universal approximators. Neural Netw. 2, 359–366. http://dx.doi.org/10.1016/0893-6080(89)90020-8.

Karakalas, A.A., Machairas, T.T., Saravanos, D.A., 2019. Effect of shape memory alloys partial transformation on the response of morphing structures encompassing shape memory alloy wire actuators. J. Intell. Mater. Syst. Struct. 30, 1682–1698. http://dx.doi.org/10.1177/1045389X19844008.

Khalil, H.K., Grizzle, J., 2002. Nonlinear systems, volume 3, Prentice hall Upper Saddle River, NJ.

Lagoudas, D.C., 2008. Shape memory alloys: Modeling and engineering applications. http://dx.doi.org/10.1007/978-0-387-47685-8.

Lezgy-Nazargah, M., Yaylacı, M., Shad, H., 2025. Double superposition shear deformation theory for buckling analysis of layered composite circular closed cylindrical shells in underwater environments. Ocean Eng. 340, 122230. http://dx.doi.org/10.1016/j.oceaneng.2025.122230.

Lima, G.S., Savi, M.A., Bessa, W.M., 2023. Intelligent control of cardiac rhythms using artificial neural networks. Nonlinear Dynam. 111, 11543–11557. http://dx.doi.org/10.1007/s11071-023-08447-1.

Liu, C., Wen, G., Zhao, Z., Sedaghati, R., 2020. Neural-network-based sliding-mode control of an uncertain robot using dynamic model approximated switching gain. IEEE Trans. Cybern. 51, 2339–2346. http://dx.doi.org/10.1109/TCYB.2020.2978003.

Liu, K., Wu, Y., Zhu, T., Chen, Y., Lu, Y., Zhao, D., 2019. Improved rbf network torque control in flexible manipulator actuated by pmas. Robotica 37, 264–280. http://dx.doi.org/10.1017/S0263574718001005.

Lü, X., Rong, K., Tian, L., Qiu, C., Du, J., 2021. Studies on the damping mechanism of shape memory alloy-spring tuned vibration absorber attached to a multi-degree-of-freedom structure. J. Vib. Control 28, 2666–2677. http://dx.doi.org/10.1177/10775463211018526.

Mamdani, E.H., 1974. Application of fuzzy algorithms for control of simple dynamic plant. In: Proceedings of the Institution of Electrical Engineers. IET, pp. 1585–1588. http://dx.doi.org/10.1049/piee.1974.0328.

Mohd Jani, J., Leary, M., Subic, A., 2017. Designing shape memory alloy linear actuators: A review. J. Intell. Mater. Syst. Struct. 28, 1699–1718. http://dx.doi.org/10.1177/1045389X1667929.

Mohd Jani, J., Leary, M., Subic, A., Gibson, M.A., 2014. A review of shape memory alloy research, applications and opportunities. Mater. Des. 56, 1078–1113. http://dx.doi.org/10.1016/j.matdes.2013.11.084.

Nespoli, A., Bassani, E., Della Torre, D., Donnini, R., Villa, E., Passaretti, F., 2017. An experimental study on pseudoelasticity of a niti-based damper for civil applications. Smart Mater. Struct. 26, 105041. http://dx.doi.org/10.1088/1361-665X/aa882e.

Niu, M.Q., Chen, L.Q., 2021. Nonlinear vibration isolation via a nitinol wire rope. Appl. Sci. 11, 10032. http://dx.doi.org/10.3390/app112110032.

Orlando, D., de Castro, C.H.L., Gonçalves, P.B., 2018. Nonlinear vibrations and instability of a bistable shallow reticulated truss. Nonlinear Dynam. 94, 1479–1499. http://dx.doi.org/10.1007/s11071-018-4437-1.

Ortiz, M., Pinsky, P.M., Taylor, R.L., 1983. Operator split methods for the numerical solution of the elastoplastic dynamic problem. Comput. Methods Appl. Mech. Engrg. 39, 137–157. http://dx.doi.org/10.1016/0045-7825(83)90018-X.

Paiva, A., Savi, M.A., 2006. An overview of constitutive models for shape memory alloys. Math. Probl. Eng. 2006, http://dx.doi.org/10.1155/MPE/2006/56876.

Paiva, A., Savi, M.A., Braga, A.M.B., Pacheco, P.M.C.L., 2005. A constitutive model for shape memory alloys considering tensile-compressive asymmetry and plasticity. Int. J. Solids Struct. 42, 3439–3457. http://dx.doi.org/10.1016/j.ijsolstr.2004.11.006.

Parmar, U., Mishra, A., 2022. Mechanical properties of niti based shape memory alloy used in manufacturing of mars rover wheels: Short review. Mater. Charact. http://dx.doi.org/10.46632/mc/1/2/9.

de Paula, A.S., Savi, M.A., 2011. Comparative analysis of chaos control methods: a mechanical system case study. Int. J. Nonlinear Mech. 46, 1076–1089. http://dx.doi.org/10.1016/j.ijnonlinmec.2011.04.031.

Pelliciari, M., Tarantino, A.M., 2020. Equilibrium paths for von mises trusses in finite elasticity. J. Elasticity 138, 145–168. http://dx.doi.org/10.1007/s10659-019-09731-1.

Qian, H., Li, H., Song, G., 2016. Experimental investigations of building structure with a superelastic shape memory alloy friction damper subject to seismic loads. Smart Mater. Struct. 25, 125026. http://dx.doi.org/10.1088/0964-1726/25/12/125026.

Rockafellar, R.T., 1970. Convex Analysis. Princeton University Press.

Santana, M.V.B., Gonçalves, P.B., Silveira, R.A.d.M., 2019. Stability and load capacity of an elasto-plastic pyramidal truss. Int. J. Solids Struct. 171, 158–173. http://dx.doi.org/10.1016/j.ijsolstr.2019.04.011.

Savi, M.A., 2015. Nonlinear dynamics and chaos in shape memory alloy systems. Int. J. Non-Linear Mech. 70, 2–19. http://dx.doi.org/10.1016/j.ijnonlinmec.2014.06.001.

Savi, M., Braga, A., 1993. Chaotic vibrations of an oscillator with shape memory. J. Braz. Soc. Mech. Sci. Eng 15, 1–20.

Savi, M.A., Nogueira, J.B., 2010. Nonlinear dynamics and chaos in a pseudoelastic two-bar truss. Smart Mater. Struct. 19, 115022. http://dx.doi.org/10.1088/0964-1726/19/11/115022.

Savi, M.A., Pacheco, P.M.C.L., Braga, A.M.B., 2002. Chaos in a shape memory two-bar truss. Int. J. Non-Linear Mech. 37, 1387–1392. http://dx.doi.org/10.1016/S0020-7462(02)00029-X.

Savi, M.A., Paiva, A., 2005. Describing internal subloops due to incomplete phase transformations in shape memory alloys. Arch. Appl. Mech. 74, 637–647. http://dx.doi.org/10.1007/s00419-005-0385-6.

Savi, M.A., Sá, M.A., Paiva, A., Pacheco, P.M., 2008. Tensile-compressive asymmetry influence on shape memory alloy system dynamics. Chaos Solitons Fractals 36, 828–842. http://dx.doi.org/10.1016/j.chaos.2006.09.043.

Scarselli, F., Tsoi, A.C., 1998. Universal approximation using feedforward neural networks: A survey of some existing methods, and some new results. Neural Netw. 11, 15–37. http://dx.doi.org/10.1016/S0893-6080(97)00097-X.

Sekban, D.M., Aktarer, S.M., Ozdemir, M.E., Yaylaci, E.U., Pirim, A.E., Kolahchi, R., Yaylaci, M., 2025. Investigation of the effect of changes in material values of fsped al5754 on contact mechanics. Adv. Nano Res. 19, 117–127. http://dx.doi.org/10.12989/anr.2025.19.2.117.

Sitnikova, E., Pavlovskaia, E., Ing, J., Wiercigroch, M., 2012. Suppressing nonlinear resonances in an impact oscillator using smas. Smart Mater. Struct. 21, 075028. http://dx.doi.org/10.1088/0964-1726/21/7/075028.

Slotine, J.J.E., Li, W., 1991. Applied Nonlinear Control. Prentice Hall.

Sohn, J.W., Ruth, J.S., Yuk, D.G., Choi, S.B., 2023. Application of shape memory alloy actuators to vibration and motion control of structural systems: A review. Appl. Sci. 13, 995. http://dx.doi.org/10.3390/app13020995.

Song, M., Luan, C., Wang, J., Yuan, L., Zhou, Z., 2022. Mechanical properties of engineering cement-based materials containing modified shape memory alloy fiber. Null doi:null.

Su, X., Xu, Y., Yang, X., 2022. Neural network adaptive sliding mode control without overestimation for a maglev system. Mech. Syst. Signal Process. 168, 108661. http://dx.doi.org/10.1016/j.ymssp.2021.108661.

Suhail, R., Amato, G., McCrum, D., 2021. Thermo-mechanical characterisation of niti-based shape memory alloy wires for civil engineering applications. J. Intell. Mater. Syst. Struct. http://dx.doi.org/10.1177/1045389x211001437.

Sutton, R.S., Barto, A.G., et al., 1998. Reinforcement Learning: An Introduction, volume 1, MIT press Cambridge.

Tian, L., Collins, C., 2005. Adaptive neuro-fuzzy control of a flexible manipulator. Mechatronics 15, 1305–1320. http://dx.doi.org/10.1016/j.mechatronics.2005.02.001.

Yaylacı, M., Yazıcıoğlu, A., Yaylacı, E.U., Terzi, M., Birinci, A., 2025. Evaluation of the contact problem of two layers one of functionally graded, loaded by circular rigid block and resting on a pasternak foundation by analytical and numerical (fem and mlp) methods. Arch. Appl. Mech. 95, 78. http://dx.doi.org/10.1007/s00419-025-02787-7.

Yazıcıoğlu, A., Yaylacı, M., Sekban, D.M., Kuleyin, H., Yaylacı, E.U., Birinci, A., Mahmoud, S.R., 2025. Analysis of the contact problem functionally graded layer placed on a pasternak foundation. ZAMM-Journal Appl. Math. Mechanics/Zeitschrift Für Angew. Math. Und Mech. 105, e70152. http://dx.doi.org/10.1002/zamm.70152.

Zhang, Y., Chen, X., Li, D., Zang, J., 2022a. Aeroelastic properties and nonlinear vibration control of a simply-supported lattice sandwich beam embedded with nitinol-steel wire ropes. Acta Mech. Solida Sin. 35, 755–764. http://dx.doi.org/10.1007/s10338-022-00318-3.

Zhang, Z.X., Zhang, J., Wu, H., Ji, Y., Kumar, D.D., 2022b. Iron-based shape memory alloys in construction: research, applications and opportunities. Materials 15, 1723. http://dx.doi.org/10.3390/ma15051723.

Zheng, L.H., Zhang, Y.W., Ding, H., Chen, L.Q., 2021. Nonlinear vibration suppression of composite laminated beam embedded with nitinol-steel wire ropes. Nonlinear Dynam. 103, 2391–2407. http://dx.doi.org/10.1007/s11071-021-06258-w.